analytical chemistry

ARTICLE

pubs.acs.org/ac

Monitoring a Reaction at Submillisecond Resolution in Picoliter Volumes

Ansgar M. Huebner,[†,‡] Chris Abell,[‡] Wilhelm T. S. Huck,[‡,∥] Charles N. Baroud,[*,§] and Florian Hollfelder[*,†]

[†]Department of Biochemistry, University of Cambridge, Cambridge CB2 1GA, United Kingdom

[‡]Department of Chemistry, University of Cambridge, Cambridge CB2 1EW, United Kingdom

[§]Laboratoire d'Hydrodynamique and Department of Mechanics (LadHyX), Ecole Polytechnique, CNRS, F-91128 Palaiseau, Cedex, France

Supporting Information

ABSTRACT: Well-established rapid mixing techniques such as stopped-flow have been used to push the dead time for kinetic experiments down to a few milliseconds. However, very fast reactions are difficult to resolve below this limit. We now outline an approach that provides access to ultrafast kinetics but does not rely on active mixing at all. Here, the reagents are compartmentalized into water-in-oil emulsion microdroplets (diameter ~50 μm) that are statically arrayed in pairs, resting side-by-side in a well feature of a poly(dimethylsiloxane) (PDMS) device. A reaction between the contents of two droplets arrayed in such a holding trap is initiated by droplet fusion that is brought about by electrocoalescence and known to occur on a time scale of about 100 μs. A reaction between the reactants (Fe^{3+} and SCN^-) is monitored by image analysis measuring the product formation in the newly merged drop in both space and time, by use of a fast camera. A comparison of the concentration field of the reaction product with the output of a reaction-diffusion system of equations yields a rate constant $k \sim 3 \times 10^4\ M^{-3} \cdot s^{-1}$. Since reaction and diffusion are formally included in the mathematical model, measurements can proceed immediately after the drop fusion, removing the need to allow time for mixing. This approach is different from existing methodologies, for example, experiments in a conventional stopped-flow apparatus but also electrofusion of moving droplets where contents are mixed by chaotic advection before a reaction is monitored. Our analysis makes kinetics accessible that are several times faster than techniques that have to allow time for mixing.

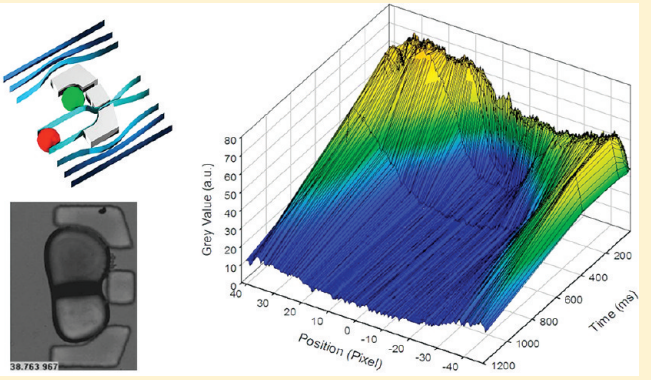

The experimental determination of reaction rates forms the basis for deriving quantitative analysis of molecular processes. Challenges in this regard include the measurement of ultrafast reactions while working with minimal amounts of reagent, be it enzyme or small molecule. Traditional techniques such as continuous and stopped-flow, T-jump, or quenched-flow give access to reaction times in the microsecond range but require substantial amounts of reagents. Microfluidic systems offer a format to reduce the amount of sample used. However, combining the advantages of both approaches has not been straightforward, in part due to the slow mixing times in laminar flows, which limit the shortest times over which a reaction can be observed. Here, we present a novel approach to overcome these constraints, which allows us to measure submillisecond reaction kinetics while requiring only picoliter volumes of reagents.

Previously the laminar nature of microfluidic flows and the typical flattened geometry of microchannels were invoked to build a model in which the growth in space of the reaction zone between two coflowing streams was used to derive kinetic information.[1] In this approach, no active mixing takes place and extraction of the chemical kinetics relies on mathematical deconvolution of the chemical reaction process from the diffusion of the species involved. The solution of an analytical reaction-diffusion (RD) model is then compared with image data that provide spatial information on product concentration in space, to yield a rate constant. While this technique begins to take advantage of some favorable microfluidics scalings, it still faces major hurdles as a consequence of its reliance on a continuous flow of reagents: Three dimensional dispersion and entrance effects of the flow in the microchannels significantly reduce the precision of the measurements at early time points.[2] In addition, continuous flow, albeit at the microscale, can still consume substantial amount of reagents[3] and makes variation of large numbers of parameters (e.g., in combinatorial experiments) impractical by requiring an unwieldy number of independent channels.

In parallel, the emerging format of water-in-oil droplet compartments has also been proposed for the measurement of chemical reactions.[4−9] In this format, reactants can be placed in contact

Received: December 10, 2010
Accepted: December 11, 2010
Published: January 18, 2011

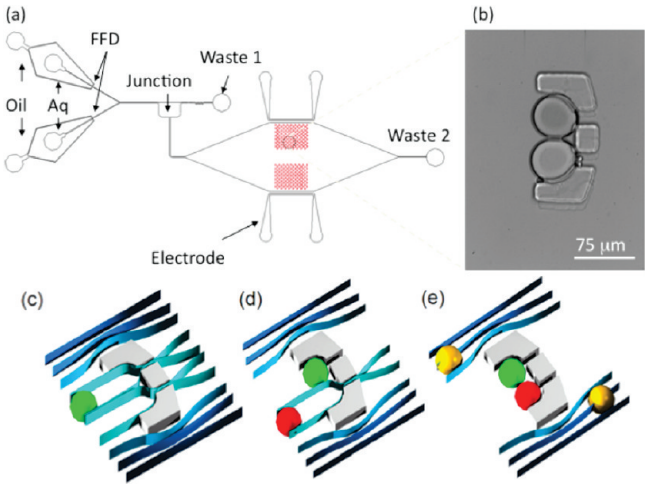

Figure 1. Double droplet trap array. (a) Schematic overview: the device (approximate total length 5 cm) includes inlets for oil and aqueous (Aq) phases, arranged in a flow focusing geometry (FFD) for droplet formation. After formation, droplets are directed either into Waste 1 or into the array (red) via a reservoir junction. Initially heterogeneous droplets were directed into Waste 1 by infusing oil via Waste 2. When visual inspection indicated that the droplet stream had stabilized, droplets were allowed to enter the array by reversing the oil flow from Waste 2. Electrodes are placed adjacent to the trap array to trigger electrocoalescence (see Figure 2). Droplets can be removed from such arrays by reversing the flow direction.[23] (b) Bright-field image of two adjacent droplets in a trap. (c−e) Schematic representation of the process of entrapment of droplets (drawn with AutoCAD): (c) A droplet enters the trap following the flow lines. Once in the trap the droplet blocks the exhaust hole, leading to termination of flow through this side of the trap. (d) A second droplet can enter the trap only at the remaining site. (e) When both positions are occupied, other droplets pass the trap following the outer flow lines. Conditions for droplet production: 30 mL/h light mineral oil containing 2% (w/w) Span80, aqueous phase flow 10 mL/h. The diameter of droplets produced in this device was approximately 50 μm, and the channel height was designed to match the droplet size at 50 μm.

either at the point of drop formation in a T-junction[10] or in a flow focusing device,[11] where two or more streams containing the reactants meet, or by fusing two droplets together as they flow in a channel.[12] In this work, the encapsulation within the drop is always followed by a rapid mixing step involving chaotic advection of the droplet contents, after which the reaction can be observed at different locations downstream. Each of these measurements corresponds to a different reaction time after the reagents are brought together. This approach allows access to reaction time scales upward of a few milliseconds. The relative concentrations within the drop can be controlled by adjusting the flow rates of the different reactants upstream of the formation or by controlling the relative size of the merging drops. In contrast to continuous-flow microfluidics, the dispersion of reagents is prevented by compartmentalization in droplets, and a scale-down of reaction volumes into the nano- to femtoliter range is possible. In contrast to measurements, for example, in a stopped-flow apparatus, there is no dead time associated with the instrument beyond the time to mix the reagents. However, the rapid mixing is associated with a rapid transport of the drops, which limits the ability to follow a single drop in time, so one must take measurements of successive drops at varying locations instead. Rates obtained in this format consequently represent an average of many drops, particularly when measurements are required for both short and long times.

The recent development of a range of unit operations to control droplet contents in microfluidic devices[6,9] allows alternative approaches to overcome the problems described above. Droplets can be formed from single components and fused by an external stimulus such as electrocoaescence,[12−19] surface modification,[20] or localized laser-induced heating.[21,22] This capability, coupled with a simple device to hold droplets stationary, can be used to measure very fast chemical kinetics between components of two droplets by performing quantitative comparisons with the RD model, which describes the behavior of species in the case of stationary drops remarkably well. Here, droplet pairs are first arrayed on a chip and are maintained stationary by a microfabricated set of traps (Figure 1). A reaction between adjacent trapped droplets is triggered through droplet electrocoalescence and is maintained by the interdiffusion of the reacting species. In contrast to previous methods, no additional mixing takes place. The reaction is monitored by measuring the product formation in the newly merged drop in both space and time, by use of a fast camera. The reaction kinetics are then obtained by quantitative comparison of the concentration field of the reaction product with the output of the RD system of equations to yield a rate constant. Since reaction and diffusion are formally included in the mathematical model, the measurements taken immediately after the drop fusion can be rigorously interpreted, removing the need to allow time for mixing or applying an empirical correction function. This approach provides access to kinetics that can be more than an order of magnitude faster than stopped-flow or droplet mixing by chaotic advection, which are limited by mixing times of a few milliseconds.

EXPERIMENTAL SECTION

Device Fabrication. The devices used in this study were constructed by conventional soft lithographic techniques.[24] Briefly, a master was prepared from SU-8 2025 (Microchem Corp.) on a silicon wafer (Compart Technology Ltd.). Slygard 184 (Dow Corning) was mixed in a 10:1 (w/w) ratio of resin to cross-linker and then poured over the master. A thickness of 50 μm was achieved by adjusting the spin coater velocities in two spinning phases: an initial phase with 500 rpm for 5 s at an acceleration of 300 rpm/s and a later phase with 1650 rpm for 40 s at 300 rpm/s. After degassing, the device was cured for 6 h at 65 °C, and the poly(dimethylsiloxane) (PDMS) was cut and peeled off the master. Access holes for the tubing and for the electrodes were drilled with a biopsy punch, and the device (total length approximately 5 cm) was exposed to air plasma for 30 s (Femto Diener) and sealed onto a standard microscope glass slide (Agar Scientific). The channels were then rendered hydrophobic by baking at 65 °C for 10−12 h before use. Electrodes were fabricated afterwards by placing the device on a hot plate and heating to 130 °C. Low melting point solder wire (No. 19, Indalloy) was pushed by hand into the entrance hole. The solder melted on contact with the hot glass and filled the void space up to the exit hole. In order to facilitate contact with the electrical equipment, copper wire was inserted into the molten solder at the entrance hole. The device was left to cool to room temperature before use. Polyethylene tubing (internal diameter i.d. = 0.38 mm, Becton Dickinson) for delivery of the liquid phases was connected to glass syringes (Hamilton) and the other end was inserted into the device relying on the elastic properties of PDMS to form a seal.

Device Operation. The fluid flow was driven by syringe pumps (Harvard Apparatus PhD 2000 infusion). Light mineral oil (Sigma Aldrich) containing 2% (w/w) Span80 (Fluka) as a surfactant was

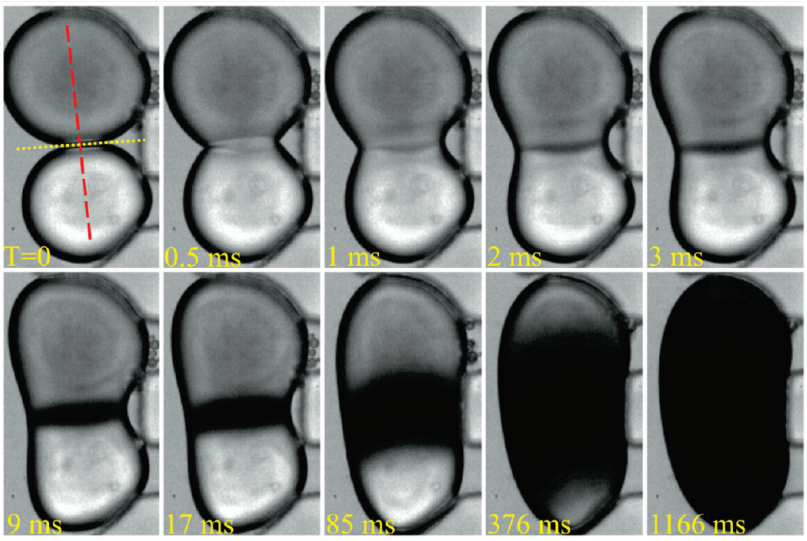

Figure 2. Complex formation triggered by electrocoalescence. The traps (Figure 1) are populated with two droplets. The contents of these droplets are randomly distributed, with about half of all droplet pairs containing the two different reactants for complex formation. The lighter colored solution in the lower droplet is KSCN (0.8 M) and the darker solution is $Fe(NO_3)_3$ (0.27 M). Upon application of an electric field the droplets merge, leading to the formation of a dark complex ($FeSCN_3$). The red line marks the axis along which the gray values (shown in Figure 3) were measured. The yellow horizontal line marks the point of contact of both droplets and defines the zero point of the axis "Position" in Figure 3. The top left image corresponds to the starting point of the reaction (T = 0), when droplets are separate. Images were taken with a fast camera (V7.2, Phantom) mounted onto a microscope (IX 71, Olympus). Temperature: 24 ± 1.5 °C.

used as the immiscible oil phase. All liquids were filtered prior to use with a filter cartridge (0.22 μm, MillexGP, Millipore). Experiments were carried out in a climatized room (24 °C) and the temperature was continuously monitored, giving a maximal temporary deviation of 1.5 °C.

Droplets were formed with two flow focusing features to produce two populations of droplets. The size of the droplets (50 μm) was chosen to match the diameter of the traps. The water fraction was kept constant at 0.25. Droplets were stored under a constant oil flow rate of 1 mL/h. As droplets formed initially were not uniform in diameter, an oil stream was infused in from Waste 2 (Figure 1) to prevent any droplets from entering the array at this stage. To allow population of the array with droplets, the oil flow from Waste 2 was reversed once the droplets were of uniform size.

Optical Methods. Droplets and the trap area were imaged on an inverted microscope (IX71, Olympus). To image droplets, a Phantom V7.2 camera was used that recorded images at 2000 Hz. Gray value analysis was carried out with ImageJ (http://rsb.info.nih.gov/ij/) and processed with SigmaPlot 8.0 and Matlab 7.4 (Mathworks).

A diode-pumped solid-state laser excitation source (Piccaro 488 nm air-cooled cyan) was fed into the microscope (IX71, Olympus) and the light beam was directed with a 40× microscope objective (UPlanFLN, Olympus) toward the trap in the microfluidic device.

Droplet Manipulation: Electrocoalescence. To fuse droplets, a square wave electric field between the electrodes was applied (430 V/mm with a frequency of 0.1 Hz). The field was brought about by a function generator (Stanford Research Systems DS335) in conjunction with a high-voltage amplifier (Trek 610E).

RESULTS

Device Design. Figure 1 shows how droplets are formed by two flow-focusing devices[25,26] and deposited in an array with 280 traps (width 100 μm) within minutes so that two droplets rest next to each other in each trap. Two exhaust channels were built through the center of each trap to ensure deposition of exactly two droplets per trap: oil passed through these exhaust channels when the trap was empty, but after droplet capture, blockage of the channel exit resulted in the reduction of liquid flow within this part of the trap (Figure 1d). After entry of the second droplet, the flow through the trap was further reduced and later droplets were prevented from entering. This mode of trapping is similar to arrays in which droplets were optically monitored[23] or the transport of small molecules across surfactant bilayers was analyzed.[27] The distribution of deposited droplets containing two reagents A and B was not controlled and was thus random, that is, approximately 50% of the traps contained homogeneous (AA or BB) and 50% contained heterogeneous (AB) droplet pairs. The ability to populate wells with two sorts of droplets offers the possibility of initiating a reaction between their contents: the two reagents can be kept apart while being arrayed and are fused at will by applying an external trigger. In the case presented here, solder electrodes adjacent to the trapping array were introduced to bring about electrocoalescence by an electric pulse, leading to simultaneous droplet fusion in all 280 wells.

Analysis of a Fast Reaction. We demonstrate that a reaction can be studied in this device design with a model chemical process involving two reagents: the colorless salts KSCN and $Fe(NO_3)_3$, which react to give a dark red complex according to

$$Fe^{3+}(aq) + xSCN^- \rightarrow Fe(SCN^-)_x^{(3-x)+}$$

Complex formation is shown in Figure 2, which displays images of a droplet pair, just after fusion, obtained with a fast camera coupled to a microscope. The progress of the reaction was monitored by recording images at a time resolution of 0.5 ms and at a spatial resolution of 0.5 μm/pixel. Complex formation begins after droplet fusion, as shown by a dark product band at the original location of the interface between the two droplets. The interdiffusion of the reacting species then makes the dark band

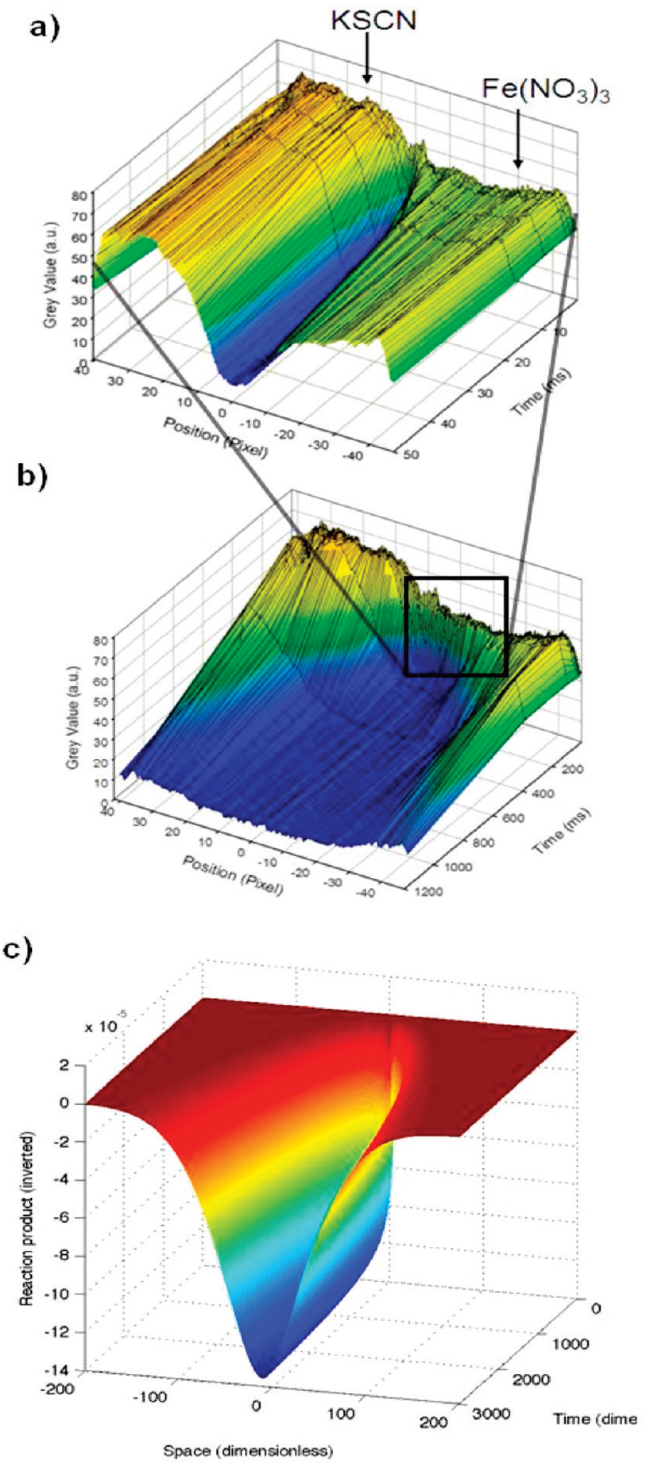

Figure 3. Experimental and calculated spatiotemporal plots of product formation. Complex formation is triggered by electrofusion and measured along the red line shown in Figure 2a. This line is perpendicular to the original interface (shown as a dotted yellow line in Figure 2a). The amount of product formed (i.e., the complex $FeSCN_3$) was derived from images (Figure 2) and is represented as the gray value. Blue corresponds to a darker pixel reading (i.e., a lower gray value) and is equivalent to a higher concentration of the complex. (a) Initial and (b) full data set of gray value as a function of time (t_0 = time of fusion) and space (origin = initial contact point of the two droplets; denoted by a red dotted line in Figure 2a). (c) Numerically simulated evolution of the concentration field of the complex, using the reaction-diffusion model discussed in the text, plotted with the same color-coding as above.

expand transversely until the whole drop is darkened after consumption of all of the reacting species (after 1 s). Product formation is initially rapid, followed by a spread across the droplet that takes place more slowly. This qualitative observation can be explained by the rapid contact of ion and ligand initially, followed by diffusion of further noncomplexed ions and ligands from increasingly larger distances. As discussed at the end of this section, the flow associated with the merging plays a minor role and can be neglected.

Product formation is measured along the transverse line shown in Figure 2. By working with transmitted white light, we may assume that the absorption of light is proportional to the concentration of the reaction product for sufficiently low concentrations. This assumption of dilute solution is reasonable at the initial stages of the reaction or near the edges of the reacting zone. Figure 3 represents product concentration as a function of time and space, along the line shown in Figure 2. Blue corresponds to a darker pixel reading (the gray value) or equivalently to a higher concentration of the complex. Starting from the first image after fusion, that is, 500 μs after placing the drop contents in contact, a steep decrease in gray values is detectable where ligand and ion meet, resulting in a dark band. The broadening of this band in the drops (Figure 2) translates into the broadening of the blue region as time advances in Figure 3. The asymmetry in the shape of the product concentration is mainly due to the unequal diffusion coefficients of ion and ligand, meaning that one will diffuse faster than the other. As a result, more product is formed in the region of the slower diffusing Fe^{3+} species.

A Quantitative Model of Reaction Progress. To disentangle transport phenomena from reaction progress, a model that includes molecular diffusion and complex formation was constructed for this reaction-diffusion problem. Such models assume that the reaction progress at every point in space is determined by the local reactant concentration. In this way, the reaction terms in the equations can be decoupled from the diffusion terms, which then provide only the transport of the different species in order to maintain the reaction progress. The evolution of the concentration of the different species therefore depends independently on the rate at which the reactants are brought in contact, through diffusion, and the rate at which they are spent, through reaction. Such RD models have attracted the interest of physical chemists, with the theoretical work generally dealing with the long time asymptotics of the reaction zone.[28] Recently, generalizations of the RD models have been developed for complex stoichiometries, with a general form of $n\mathrm{A} + m\mathrm{B} \rightarrow \mathrm{C}$.[29] In such models, the rates of consumption of the species A and B are given by $R_A = nkA^nB^m$ and $R_B = mkA^nB^m$, respectively, and the rate of production of C is $R_C = kA^nB^m$. Here $A(x,t)$, $B(x,t)$, and $C(x,t)$ are the concentrations of the two reagents and the product, which are allowed to vary along one space dimension and time, and k is the traditional reaction rate constant, which is unique for a given combination of reagents. For the stoichiometry of the current experiment, we use $n = 1$ and $m = 3$. The reaction-diffusion model equations can be written as

$$\begin{aligned} \partial_t A &= D_A \partial_{xx} A - R_A \\ \partial_t B &= D_B \partial_{xx} B - R_B \\ \partial_t C &= D_C \partial_{xx} C + R_C \end{aligned} \qquad (1)$$

where ∂_t is the time derivative, ∂_{xx} is a second derivative in space, and D_A, D_B, and D_C are the diffusion coefficients of the three species. In this model, the left-hand side of the equations describes the time evolution of each of the species at every point in space and time. The first term on the right-hand side describes the diffusion of each species by Brownian motion, while the last term accounts for

dx.doi.org/10.1021/ac103234a |*Anal. Chem.* 2011, 83, 1462–1468

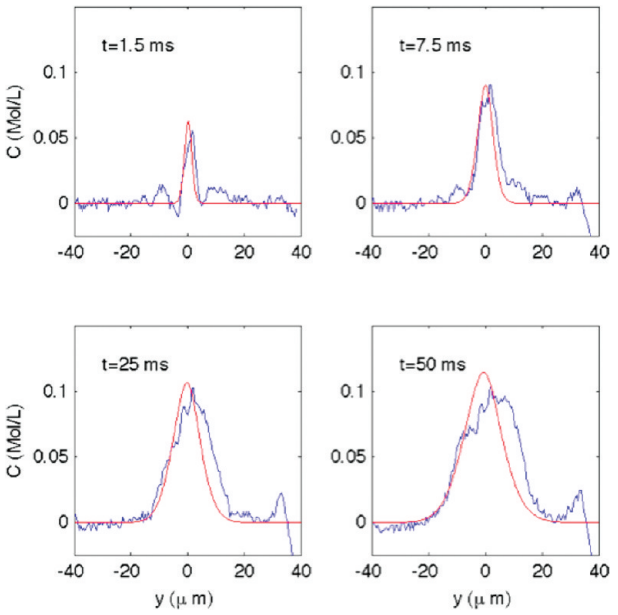

Figure 4. Comparison between numerical solution and experimental measurement. Product formation is monitored by measuring the gray levels on the experimental images (Figure 2) and is shown by the blue curves at four characteristic times. The red curves show the numerically calculated values of the reaction product at the same times, using the best fitting value of the reaction kinetic constant.

the depletion of A and B or production of C, as a result of the reaction progress.

These equations are first nondimensionalized by introducing a characteristic time scale $[\tau = 1/(kA_0B_0^2)]$ and length scale L [such that $L^2 = (D_AD_B)^{1/2}/(kA_0B_0^2)$] where A_0 and B_0 are the known initial concentrations of each of the reacting species in their respective droplets. The details of the mathematical treatment are outlined in the Supporting Information. The dimensionless form of the model is then solved numerically to yield the concentration profile shown in Figure 3c, where the blue regions correspond to high concentrations of the reaction product. The numerical and experimental fields should match each other when τ and L^2 are correctly chosen in order to differentially stretch the space and time axes in Figure 3c. This corresponds to choosing the correct value of k, the other quantities being known in our case. All quantities in eq 1 will be affected by this stretching, since all of the concentrations depend on both time and space. For this reason, fitting one of the measurable parameters will yield good agreement for the other parameters only if the system of equations indeed describes the underlying process correctly.

We chose to obtain the value of k by measuring the increase in time of the maximum product concentration and comparing the numerics and experiments. This fit (shown in the Supporting Information) yields $k \sim 3 \times 10^4\ M^{-3}\cdot s^{-1}$, with an uncertainty of 20%.[30−33] This value of k is used to calculate the variables $\tau = 200\ \mu s$ and $L = 0.5\ \mu m$, in order to rescale the dimensionless solution onto dimensional variables and compare with the experimentally measured profiles. This comparison is shown in Figure 4, where the theoretical and experimental concentration profiles are superimposed for four discrete times. At early time points the fit represents the data very well, while deviation increases as time progresses. This is consistent with the hypothesis that the gray value represents the product concentration, which may hold only for low concentrations, that is, at early times. Nevertheless, the good agreement that is exhibited by the two sets of curves supports the validity of the RD model which captures not only the value of the maximum concentration but also the width and shape of the concentration profile.

The coalescence of the two drops involves a flow of fluids that is not accounted for in the RD model. This advective movement can be divided into two distinct regimes. The velocities in these regimes can be estimated from Figure 2: At early time points (below t = 2 ms), the drop shape undergoes large changes in the vicinity of the initial interface position but remains unchanged far away from the interface. Then, for late time points, the drop globally relaxes to its final shape over the course of about 100 ms.

The effect of the initial fast flow is to redistribute the drop contents during the merging process. However, since the two drops are of equal viscosities and surface tensions, this flow is directed parallel to the interface, since it is determined by a balance of the surface tension and local viscous shear. Therefore, no active mixing should take place between the initially separated species but the two reagents are expected to remain well separated after this process. The flow arising from this separation is damped over a time scale given by the viscous diffusion time, $T \sim L^2/\nu$, where $L \sim 10\ \mu m$ is a characteristic length scale and the kinematic viscosity ν is nearly 20 times the water viscosity. This calculation yields a value of T on the order of 0.1 ms, implying that the initial flow is damped within 100 μs in our system. This analysis suggests that no further recirculation takes place once the interfaces are merged.

On the long time scale, the relaxation of the drop to its final shape is associated with a flow velocity on the order of 10 μm/100 ms. During the 20 ms over which the fit between the model and the experiment is performed, the relaxation corresponds to an advective motion of around 2 μm, to be compared with the observed broadening of the profile, which covers more than 20 μm. We therefore conclude that the error induced by the flow within the droplets can safely be neglected for the geometry and fluids in our study, justifying the use of a pure reaction-diffusion model. Finally, the width of the dark region can be measured as a function of time and yields a broadening that is close to a $t^{1/2}$ dependence for a wide range of time scales (Supporting Information, Figure S1). This further confirms that the transport mechanisms are dominated by diffusion.

DISCUSSION AND CONCLUSIONS

This methodology provides a new approach to measuring rapid kinetics, using extremely small volumes. A simple device and basic microfluidic equipment is used to array droplet pairs, electrocoalescence triggers the contact between droplet contents, and an optical readout is used to determine diffusion and reaction. In fitting the simulations and experiments we obtain the time scale τ, which characterizes the time necessary for the concentrations to vary due to the reaction, in addition to L, which measures the characteristic distance over which species have diffused during this time. A key point is that chemical kinetics faster than the camera frame rate become accessible by the fitting procedure. This is possible only because the same physical processes—namely, reaction and diffusion—are operating from the beginning to the end of the experiment, in contrast with other methods where the reaction is observed only after an initial mixing step.

When compared to single-phase microfluidic coflow systems,[1,34,35] droplet fusion solves the problems associated with the parabolic flow, in addition to yielding a well-defined starting point for the reaction, because reagents are held apart by the droplet compartments prior to initiation by the fusion. Indeed, droplet merging occurs over a time of

about 100 μs,[14] which should be compared with the time for the fluid to pass the entrance length in coflow systems, estimated at 4.5 ms.[34] If necessary, the fusion time can be further reduced by modifying the geometry of the traps, using fluids with higher interfacial tension, or using smaller droplets.[36] Thus the limit of time scales potentially accessible for the measurements of chemical kinetics is lowered substantially compared with current microfluidics approaches, which are limited to a few milliseconds. The data quality can be further improved by using more sensitive fluorescence detection and averaging over several fusion events.

The immobilization of droplets precludes artifacts related to advection, which are encountered in flowing droplets or coflow systems.[2] Indeed, while single-phase flows suffer from parabolic velocity fields, deconvoluting the mixing profile for chaotic advection at the level of an individual moving droplet is nontrivial and even impossible for weak signals.[37] These issues do not arise when stationary droplets and image analysis are used as outlined in this study. Furthermore, constraints arising from the viscosity of solutions that do not mix well (e.g., in studies of polymers or viscous biological media) are removed: as long as the diffusion coefficient of the molecules studied is known, the formalism of the RD system can be applied.

Access to very fast reaction times by use of extremely small volumes harbors the potential for future use in a range of potential applications. For example, higher resolution of fast processes on the submillisecond time scale involving proteins or single cells[38,39] may reveal kinetic complexities that are currently undetectable and lead to mechanistic insight in catalysis or folding experiments. It is conceivable to extend this format to combinatorial library screening experiments that have recently been demonstrated in microdroplets.[40,41] Libraries in which each droplet contains a library member encoded by a fluorescent dye[40] could be interrogated on a time scale that is not amenable to conventional screening approaches. In such an approach, a library of drops can be produced separately and stored off-chip, before being reinjected into a device such as described here. About 100 droplets can be monitored in parallel when all droplets are fused simultaneously after electrocoalescence triggers reaction. Alternatively, droplets can be successively fused by laser irradiation.[42]

The simple device design and operation, conservation of sample in picoliter droplet volumes, and the ability to rapidly and reliably vary the reaction components supplied by microfluidic channels should make this methodology an attractive approach to measuring precise ultrafast kinetics.

■ ASSOCIATED CONTENT

Supporting Information. Eight figures and additional text describing derivation of the reaction-diffusion model. This material is available free of charge via the Internet at http://pubs.acs.org.

■ AUTHOR INFORMATION

Corresponding Author

*E-mail: baroud@ladhyx.polytechnique.fr (C.N.B.) or fh111@cam.ac.uk (F.H.).

Present Addresses

[||]Radboud University Nijmegen, Institute for Molecules and Materials, Heyendaalseweg 135, 6525 AJ Nijmegen, The Netherlands.

■ ACKNOWLEDGMENT

This work was supported by the RCUK Basic Technology Programme and the EU NEST Project MiFem. A.H. was supported a fellowship from the EU FP6 Early Stage Training Site ChemBioChem. F.H. is an ERC Starting Investigator. We thank Yolanda Schaerli for a critical reading of the manuscript.

■ REFERENCES

(1) Baroud, C. N.; Okkels, F.; Menetrier, L.; Tabeling, P. *Phys. Rev. E: Stat., Nonlinear, Soft Matter Phys.* **2003,** *67* (6 Pt 1), No. 060104.

(2) Ismagilov, R. F.; Stroock, A. D.; Kenis, P. J. A.; Whitesides, G.; Stone, H. A. *Appl. Phys. Lett.* **2000,** *76* (17), 2376–2378.

(3) Pollack, L.; Tate, M. W.; Darnton, N. C.; Knight, J. B.; Gruner, S. M.; Eaton, W. A.; Austin, R. H. *Proc. Natl. Acad. Sci. U.S.A.* **1999,** *96* (18), 10115–10117.

(4) Song, H.; Chen, D. L.; Ismagilov, R. F. *Angew. Chem., Int. Ed.* **2006,** *45* (44), 7336–7356.

(5) Huebner, A.; Sharma, S.; Srisa-Art, M.; Hollfelder, F.; Edel, J. B.; DeMello, A. J. *Lab Chip* **2008,** *8* (8), 1244–1254.

(6) Schaerli, Y.; Hollfelder, F. *Mol. Biosyst.* **2009,** *5*, 1392–1404.

(7) Teh, S.-Y.; Lin, R.; Hung, L.-H.; Lee, A. P. *Lab Chip* **2008,** *8* (2), 198–220.

(8) Theberge, A. B.; Courtois, F.; Schaerli, Y.; Fischlechner, M.; Abell, C.; Hollfelder, F.; Huck, W. T. *Angew. Chem., Int. Ed.* **2010,** *49* (34), 5846–5868.

(9) Kintses, B.; van Vliet, L.; Devenish, S.; Hollfelder, F. *Curr. Opin. Chem. Biol.* **2010,** *i14* (5), 548–555.

(10) Song, H.; Ismagilov, R. F. *J. Am. Chem. Soc.* **2003,** *125* (47), 14613–14619.

(11) Huebner, A.; Olguin, L. F.; Bratton, D.; Whyte, G.; Huck, W. T. S.; de Mello, A. J.; Edel, J. B.; Abell, C.; Hollfelder, F. *Anal. Chem.* **2008,** *80* (10), 3890–3896.

(12) Ahn, K.; Agresti, J. J.; Chong, H.; Marquez, M.; Weitz, D. A. *Appl. Phys. Lett.* **2006,** *88* (26), No. 264105.

(13) Link, D. R.; Grasland-Mongrain, E.; Duri, A.; Sarrazin, F.; Cheng, Z.; Cristobal, G.; Marquez, M.; Weitz, D. A. *Angew. Chem., Int. Ed.* **2006,** *45* (16), 2556–2560.

(14) Priest, C.; Herminghaus, S.; Seemann, R. *Appl. Phys. Lett.* **2006,** *89* (13), No. 134101.

(15) Chabert, M.; Dorfman, K. D.; Viovy, J. L. *Electrophoresis* **2005,** *26* (19), 3706–3715.

(16) Zagnoni, M.; Cooper, J. M. *Lab Chip* **2009,** *9* (18), 2652–2658.

(17) Niu, X.; Gielen, F.; deMello, A. J.; Edel, J. B. *Anal. Chem.* **2009,** *81* (17), 7321–7325.

(18) Zagnoni, M.; Le Lain, G.; Cooper, J. M. *Langmuir* **2010,** *26* (18), 14443–14449.

(19) Mazutis, L.; Baret, J. C.; Treacy, P.; Skhiri, Y.; Araghi, A. F.; Ryckelynck, M.; Taly, V.; Griffiths, A. D. *Lab Chip* **2009,** *9* (20), 2902–2908.

(20) Fidalgo, L. M.; Abell, C.; Huck, W. T. S. *Lab Chip* **2007,** *7* (8), 984–986.

(21) Baroud, C. N.; de Saint Vincent, M. R.; Delville, J. P. *Lab Chip* **2007,** *7* (8), 1029–1033.

(22) Verneuil, E.; Cordero, M.; Gallaire, F.; Baroud, C. N. *Langmuir* **2009,** *25* (9), 5127–5134.

(23) Huebner, A.; Bratton, D.; Whyte, G.; Yang, M.; Demello, A. J.; Abell, C.; Hollfelder, F. *Lab Chip* **2009,** *9* (5), 692–698.

(24) Whitesides, G. M.; Ostuni, E.; Takayama, S.; Jiang, X.; Ingber, D. E. *Annu. Rev. Biomed. Eng.* **2001,** *3*, 335–373.

(25) Anna, S. L.; Bontoux, N.; Stone, H. A. *Appl. Phys. Lett.* **2003,** *82* (3), 364–366.

(26) Ward, T.; Faivre, M.; Abkarian, M.; Stone, H. A. *Electrophoresis* **2005,** *26* (19), 3716–3724.

(27) Bai, Y.; He, X.; Liu, D.; Patil, S. N.; Bratton, D.; Huebner, H.; Hollfelder, F.; Abell, C.; Huck, W. T. S. *Lab Chip* **2010,** *10* (10), 1281–1285.

(28) Galfi, L.; Racz, Z. *Phys. Rev. A* **1988,** *38* (6), 3151–3154.
(29) Trevelyan, P. M.; Strier, D. E.; De Wit, A. *Phys. Rev. E: Stat., Nonlinear, Soft Matter Phys.* **2008,** *78* (2 Pt 2), No. 026122.
(30) Below, J. F., Jr.; Connick, R. E.; Coppel, C. P. *J. Am. Chem. Soc.* **1958,** *80* (12), 2961–2967.
(31) Funahashi, S.; Ishihara, K.; Tanaka, M. *Inorg. Chem.* **1983,** *22* (14), 2070–2073.
(32) Doss, R.; Van Eldik, R.; Kelm, H. *Ber. Bunsen-Ges.* **1982,** *86*, 925.
(33) To the best of our knowledge there is no direct comparison for this rate constant on record in the literature. Previous measurements were taken under different conditions of pH and pressure, under which intermediate mono- or dithiocyanate complexes were formed.[30−32] In addition, different groups report diverging results.[31,32] By contrast, our data can be fit cleanly to a third-order rate law, while alternative fits are considerably worse.
(34) Salmon, J. B.; Dubrocq, C.; Tabeling, P.; Charier, S.; Alcor, D.; Jullien, L.; Ferrage, F. *Anal. Chem.* **2005,** *77* (11), 3417–3424.
(35) Ristenpart, W. D.; Wan, J. D.; Stone, H. A. *Anal. Chem.* **2008,** *80* (9), 3270–3276.
(36) Baroud, C. N.; Gallaire, F.; Dangla, R. *Lab Chip* **2010,** *10* (16), 2032–2045.
(37) Srisa-Art, M.; deMello, A. J.; Edel, J. B. *Anal. Chem.* **2007,** *79* (17), 6682–6689.
(38) A cell would not diffuse significantly and can therefore be considered static while the diffusion of a reaction partner would be monitored.
(39) Shim, J. U.; Olguin, L. F.; Whyte, G.; Scott, D.; Babtie, A.; Abell, C.; Huck, W. T.; Hollfelder, F. *J. Am. Chem. Soc.* **2009,** *131* (42), 15251–15256.
(40) Brouzes, E.; Medkova, M.; Savenelli, N.; Marran, D.; Twardowski, M.; Hutchison, J. B.; Rothberg, J. M.; Link, D. R.; Perrimon, N.; Samuels, M. L. *Proc. Natl. Acad. Sci. U.S.A.* **2009,** *106* (34), 14195–14200.
(41) Agresti, J. J.; Antipov, E.; Abate, A. R.; Ahn, K.; Rowat, A. C.; Baret, J. C.; Marquez, M.; Klibanov, A. M.; Griffiths, A. D.; Weitz, D. A. *Proc. Natl. Acad. Sci. U.S.A.* **2010,** *107* (9), 4004–9.
(42) See Figure S3 (Supporting Information) for an example of laser-induced fusion in this format.